JCTC Journal of Chemical Theory and Computation

Article

pubs.acs.org/JCTC

Assessment of Empirical Models versus High-Accuracy Ab Initio Methods for Nucleobase Stacking: Evaluating the Importance of Charge Penetration

Trent M. Parker and C. David Sherrill*

Center for Computational Molecular Science and Technology, School of Chemistry and Biochemistry, and School of Computational Science and Engineering, Georgia Institute of Technology, Atlanta, Georgia 30332-0400, United States

Supporting Information

ABSTRACT: Molecular mechanics (MM) force field models have been demonstrated to have difficulty reproducing certain potential energy surfaces of π-stacked complexes. Here, we examine the performance of the AMBER and CHARMM models relative to high-quality ab initio data across systematic helical parameter scans and typical B-DNA geometries for π-stacking energies of nucleobase dimers. These force fields perform best for typical B-DNA geometries (mean absolute error < 1 kcal mol^{-1}), whereas errors typically approach ~2 kcal mol^{-1} for broader potential scans, with maximum errors > 10 kcal mol^{-1} relative to high-quality ab initio reference interaction energies. The adequate performance of MM models near minimum energy structures is accomplished through cancellation of errors in various energy terms, whereas large errors at short intermolecular distances are caused by large MM electrostatics errors due to a lack of explicit terms modeling charge penetration effects.

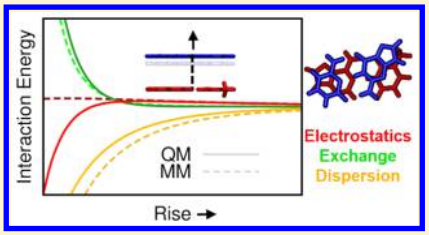

1. INTRODUCTION

Noncovalent interactions are prevalent in molecular biology and are vital to the proper functioning of biochemical pathways. These interactions govern protein folding, drug−ligand binding, intercalation, and nucleobase stacking.[1−3] Experiments that directly probe the nature of these interactions are rare, and simulations are often valuable in understanding the magnitude and preferences of these interactions.[4,5]

In recent years, computers and algorithms have advanced such that the energetics of noncovalent interactions between small molecules may be routinely computed with high accuracy.[6−9] State-of-the-art computations utilize coupled-cluster theory through perturbative triples [CCSD(T)][10] in a large, augmented basis set, with remaining basis set incompleteness corrected using a complete basis set (CBS) extrapolation from second-order Møller−Plesset perturbation theory.[11] These gold standard[12] computations can be performed for molecular systems of up to 30 or so atoms. Beyond this size, more approximate levels of theory must be used. Recently, a heirarchy of model chemistries has been developed for noncovalent interaction computations.[13−16] Two such less demanding but reliable model chemistries include spin-component scaled second-order Møller−Plesset perturbation theory for molecular interactions in the cc-pVTZ basis set [SCS(MI)-MP2/cc-pVTZ][17] and zeroth-order symmetry-adapted perturbation theory in the truncated jun-cc-pVDZ basis set (SAPT0/jun-cc-pVDZ),[18−20] which are used in this work as a good indicator of reasonably high-accuracy ab initio values, exhibiting mean absolute errors (MAE) of 0.28 and 0.32 kcal mol^{-1}, respectively, relative to CCSD(T)/CBS across the mixed and dispersion dominated subset of 345 representative bimolecular complexes.[13,14]

Biological macromolecules often contain thousands or even millions of atoms and cannot be modeled directly by ab initio quantum mechanical methods. Instead, empirical force field models are typically used.[21−26] In molecular mechanics (MM), noncovalent interactions are modeled as an electrostatic interaction between atom-centered point charges, and a Lennard-Jones potential between pairs of nonbonded atoms (see eq 1). Two of the most prevalent MM models in biophysics include AMBER[23] and CHARMM.[22] Here, we seek to understand how these simple, empirical models compare to robust high-accuracy quantum mechanics for the interactions between stacked nucleic acid base pairs.

Precise agreement between MM and QM is not to be expected for small gas-phase dimer computations. Not only are MM force fields limited in terms of the quality of the parameters and the flexibility of their underlying mathematical functions but also it is customary to deliberately build in some degree of error for pairwise interactions to partially compensate for errors caused by the lack of polarization terms in nonpolarizable force fields. Hence, an MM model may exhibit modest errors for gas-phase dimer computations and yet (due to error cancellation) perform rather well for many condensed phase properties. Nevertheless, in cases of very large errors between MM and QM, such as we see for some geometries considered in the present article, polarization effects in condensed phases will not be large enough to lead to effective error cancellation. Hence, we believe that comparisons of nonpolarizable MM energies to high-qualty QM benchmarks are valuable for gas-phase dimers because they can identify

Received: June 22, 2015
Published: August 3, 2015

DOI: 10.1021/acs.jctc.5b00588
J. Chem. Theory Comput. 2015, 11, 4197−4204

geometries where the MM errors become excessive. Moreover, in such cases, a detailed comparison to QM intermolecular interaction components (electrostatics, exchange-repulsion, etc.) may provide insight into how to create more flexible and accurate functional forms for next-generation force fields.

Previous work has examined the limitations of MM models applied to stacking of aromatic systems, particularly the benzene dimer.[27] Large errors in the electrostatics result from the inability of fixed, atom-centered point charges to model the complex charge penetration[28,29] effects of overlapping π-electron clouds (enhanced by the close contact allowed by the flat molecular surfaces). This problem is magnified in benzene due to not only the large π cloud but also the small number of unique MM parameters because of its high molecular symmetry. We have previously shown[30] that charge penetration is significant for stacked nucleobases separated by less than 4 Å, as is the case for in situ DNA double helices. Hobza and co-workers have previously examined the performance of AMBER relative to high-quality coupled-cluster stacking energies of 10 canonical nucleobase steps (nucleobase tetramers, stacked base pairs) at their average B-DNA geometries and showed reasonable accuracy (MAE < 2 kcal mol^{-1}).[31]

We seek to expand on these results by comparing MM stacking energies to high-quality ab initio results across a broad exploration of the potential energy surface of stacked nucleobase dimers and selected stacked base pairs versus several helical degrees of freedom. A thorough examination of the magnitude of these errors as well as their physical origin will aid in the development of the next-generation of force fields and address the question of whether simple functional forms are sufficient for modeling general nucleobase stacking interactions for any accessible structure.

2. THEORETICAL METHODS

The structures of canonical nucleobase pairs adenine−thymine (AT), guanine−cytosine (GC), and adenine−uracil (AU) were obtained at the B3LYP-D/aug-cc-pVDZ level of theory[32,33] in the Psi4 program.[34] For simplicity, bases and base pairs were optimized with planar exocyclic amino hydrogens. Individual nucleobase geometries (A, T, G, C, U) were then taken from these optimized base pair geometries (adenine from A−T pair). Stacked base complexes were prepared by an in-house program according to the Cambridge University Engineering Department Helix Computation Scheme (CEHS)[35] conventions for helical parameters[36] (Figure 1). Shift, Slide, and Rise represent translations relative to the *X*, *Y*, and *Z* local middle axis system, respectively (see Supporting Information).[37] Tilt, Roll, and Twist represent rotations around the *X*, *Y*, and *Z* local axes, respectively. For single bases, the local axis system is defined as the base pair axis of a base on strand I, and the origin is the nucleobase center of mass. Further details on implementation are located in the Supporting Information.

Two-dimensional potential energy surface scans of base−base stacking interactions were then performed with a grid of points in the Rise−Twist, Slide−Shift, and Tilt−Roll parameter spaces. These scans go from 0° to 180° Twist and 3.0 to 9.0 Å Rise, from −2.0 to +2.0 Å Slide and Shift, and from −20° to +20° Tilt and Roll.

To compare to canonical B-DNA structures, we also generated base steps (dimer of stacked base pairs, tetramer of nucleobases) at the average crystallographic structure (in terms of these six coordinates) of each base step from the Nucleic Acids Database (NDB).[38,39] We then computed the pairwise interaction energy (IE) between pairs of stacked nucleobases in the nucleobase tetramer comprising each base step.

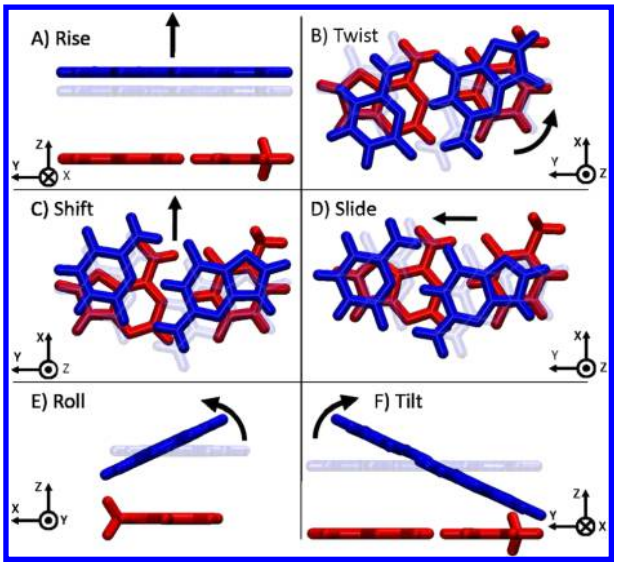

Figure 1. Example of the six nucleic acid base step structural parameters shown for the AC:GT base step (AT, red; CG, blue). Translations include Rise (+*Z*), Slide (+*Y*), and Shift (+*X*) in panels A, D, and C, respectively. Counterclockwise rotations include Twist (+*Z*), Roll (+*Y*), and Tilt (+*X*) in panels B, E, and F, respectively. The +*X* axis goes toward the major groove, +*Y* axis goes toward strand I, and +*Z* axis goes up the helix.[35,36]

MM models AMBER[23] and CHARMM[22] are often used as the potential energy function in biomodeling simulations. These force fields use nonbonded interactions of the form

$$E^{MM}_{nonbond} = \sum_{i<j}^{atoms} \epsilon_{ij}\left(\frac{R_{o,ij}}{R_{ij}^{12}} - \frac{R_{o,ij}}{R_{ij}^{6}}\right) + \frac{q_i q_j}{4\pi\epsilon_o R_{ij}} \quad (1)$$

where q_i are atomic charges and the pairwise $R_{o,ij}$ and ϵ_{ij} parameters come from atomic R_o and ϵ parameters using arithmetic and geometric combination rules, respectively. The parameters used in this study come from the most recent force field versions as of this publication, AMBER FF14[23,40,41] and CHARMM36.[42] The dielectric constant, ϵ, is set to 1. Interaction energies of stacked nucleobases at all conformations were computed using an in-house implementation of the nonbonded component of these force fields.

The gold standard level of theory, estimated CCSD(T)/CBS, is beyond the computational tractibility of the largest complexes in this study. The more tractable silver standard dispersion-weighted, explicitly correlated CCSD(T) [DW-CCSD(T**)-F12/aug-cc-pVDZ][43] typically has mean absolute errors (MAE) of 0.06 kcal mol^{-1} relative to CCSD(T)/CBS for small van der Waals dimers.[13] Here, we use DW-CCSD(T**)-F12/aug-cc-pVDZ for a limited subset of geometries (∼100) to validate the accuracy of the pewter standard[13] SCS(MI)-MP2/cc-pVTZ and bronze SAPT standard[14] SAPT0/jun-cc-pVDZ, which are used for the remainder of all geometries (∼30 000) examined here. SAPT0 and MP2 calculations were performed with Psi4, with CCSD(T)-F12 computations performed using MOLPRO.[44]

To further examine the origin of differences between MM and ab initio methods, we compute SAPT0/jun-cc-pVDZ, AMBER, and CHARMM stacking energies for nucleobase steps

DOI: 10.1021/acs.jctc.5b00588
J. Chem. Theory Comput. 2015, 11, 4197−4204

and their IE components: electrostatics, exchange-repulsion (sterics), induction (polarization, charge transfer), and London dispersion interactions. These terms are computed directly in SAPT0, and we assert the partition of MM into analogous terms: charge−charge terms as electrostatics, R^{-12} terms as exchange-repulsion, and R^{-6} terms as dispersion. These SAPT0 and MM terms are not necessarily directly equivalent, but they serve as useful indicators for error analysis.

3. RESULTS AND DISCUSSION

Figure 2 contains a comparison of stacking interaction energies for individual pairs of stacked nucleobases extracted from the

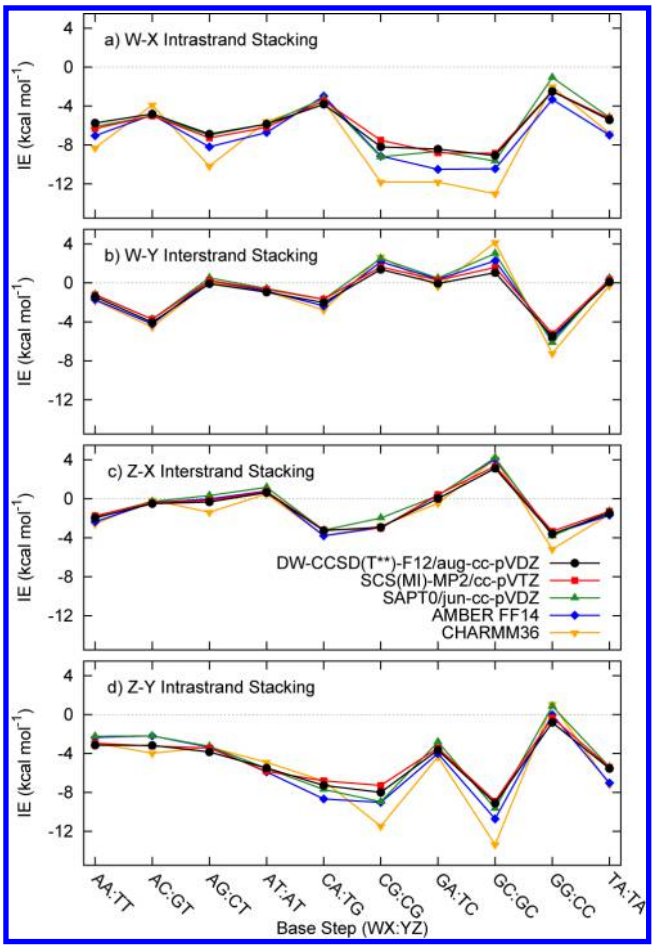

Figure 2. Comparison of stacking interaction energy computed for the 10 canonical base steps at their average B-DNA structure from the NDB.[38,39] For each base step (WX:YZ), there are four pairwise stacking interactions: two intrastrand (W−X and Z−Y) and two interstrand (W−Y and Z−X), as seen in panels a−d. Model chemistries include silver standard[13] DW-CCSD(T**)-F12/aug-cc-pVDZ, pewter standard[13] SCS(MI)-MP2/cc-pVTZ, bronze SAPT standard[14] SAPT0/jun-cc-pVDZ, and molecular mechanics force fields AMBER and CHARMM.

10 canonical base pair steps at their average B-DNA geometries in the NDB.[38,39] Against benchmark-quality DW-CCSD(T**)-F12/aug-cc-pVDZ results, we compare more approximate SCS(MI)-MP2/cc-pVTZ and SAPT0/jun-cc-pVDZ ab initio methods and also AMBER FF14 and CHARMM36.

Figure 3 compares these same methods across scans of the six helical degrees of freedom for the interaction energy in a stacked arrangement of adenine and cytosine. This figure is representative, but the Supporting Information contains similar figures for all 25 stacking combinations of the five canonical nucleobases. Figure 4 presents MAE averaged across the scans of the helical degrees of freedom for each of the 25 stacked dimers and also the MAE averaged over all 25 dimers. A further breakdown of these error statistics for the individual Rise−Twist, Slide−Shift, and Tilt−Roll potential energy surfaces (PES) is also located in the Supporting Information.

3.1. Canonical B-DNA Stacked Dimers. Computing silver standard DW-CCSD(T**)-F12/aug-cc-pVDZ interaction energies for all geometries considered here (>30 000) is intractable. Instead, a select set of representative geometries has been chosen to compare DW-CCSD(T**)-F12/aDZ and the more economical SCS(MI)-MP2/cc-pVTZ, validating use of the latter as the reference energy for the remainder of the data set. Figures 2 and 3 plot the IE's for both methods, showing an excellent agreement. Across the 40 different pairwise stacking interactions at canonical B-DNA base step parameters in Figure 2 (ranging from +3.1 to −9.1 kcal mol^{-1} reference IE), SCS(MI)-MP2/cc-pVTZ exhibits a mean absolute error (MAE) of 0.29 kcal mol^{-1} and a max error of 0.71 kcal mol^{-1}. Similarly, across a scan of all six helical parameters of adenine stacked on cytosine in Figure 3, SCS(MI)-MP2/TZ compares very well to DW-CCSD(T**)-F12/aDZ, with an MAE of 0.16 kcal mol^{-1} and max error of 0.74 kcal mol^{-1}. This good agreement across a wide set of geometries is consistent with previous studies of van der Waals dimers[13,16] and validates the use of SCS(MI)-MP2/TZ as a reference IE for the remainder of the study. The bronze SAPT standard SAPT0/jun-cc-pVDZ has an MAE of 0.57 kcal mol^{-1} and max error of 2.0 kcal mol^{-1} relative to the DW-CCSD(T**)-F12/aug-cc-pVDZ reference for these 40 interactions, which is ∼2 times that of SCS(MI)-MP2/TZ. Thus, with these higher errors, we have not chosen SAPT0 as a reference IE for this study.

The AMBER and CHARMM force fields both perform reasonably well across the 40 pairwise stacking interactions at the 10 average B-DNA base step geometries. For many base steps, this agreement is quantitative, with errors below 0.5 kcal mol^{-1} in magnitude. For others, notably, GA:TC and GC:GC, AMBER displays max errors in excess of 2 kcal mol^{-1}, whereas CHARMM is off by more than 4 kcal mol^{-1}. However, these errors do cancel somewhat across the four intrastrand and interstrand stackings interactions, leading to stacking energy errors for the entire base step that are smaller than those for the individual base−base stacking interactions. AMBER and CHARMM have MAE's of 0.67 and 1.29 kcal mol^{-1}, respectively, relative to DW-CCSD(T**)-F12/aug-cc-pVDZ, whereas each has a mean signed error (MSE) that is one-third smaller in magnitude (−0.42 and −0.82 kcal mol^{-1}, respectively), demonstrating this cancellation of error.

3.2. Base−Base Stacking Parameter Scans. Figure 3 shows the typical trends one can expect across a scan of a particular helical parameter. Long-range behavior is dominated by dispersion interactions modeled by the R^{-6} van der Waals term, as well as any molecular dipole−dipole interactions, which decay as R^{-3}. Both of these properties are modeled well in molecular mechanics, thus resulting in the good agreement between force fields and ab initio methods versus Rise at medium to long range (Rise > 4 Å). Previous work[30] has noted that charge penetration effects[28,29] become highly attractive and dominate the electrostatic contribution to the IE below 4 Å. At short range, we see significant positive deviations of MM

DOI: 10.1021/acs.jctc.5b00588
J. Chem. Theory Comput. 2015, 11, 4197−4204

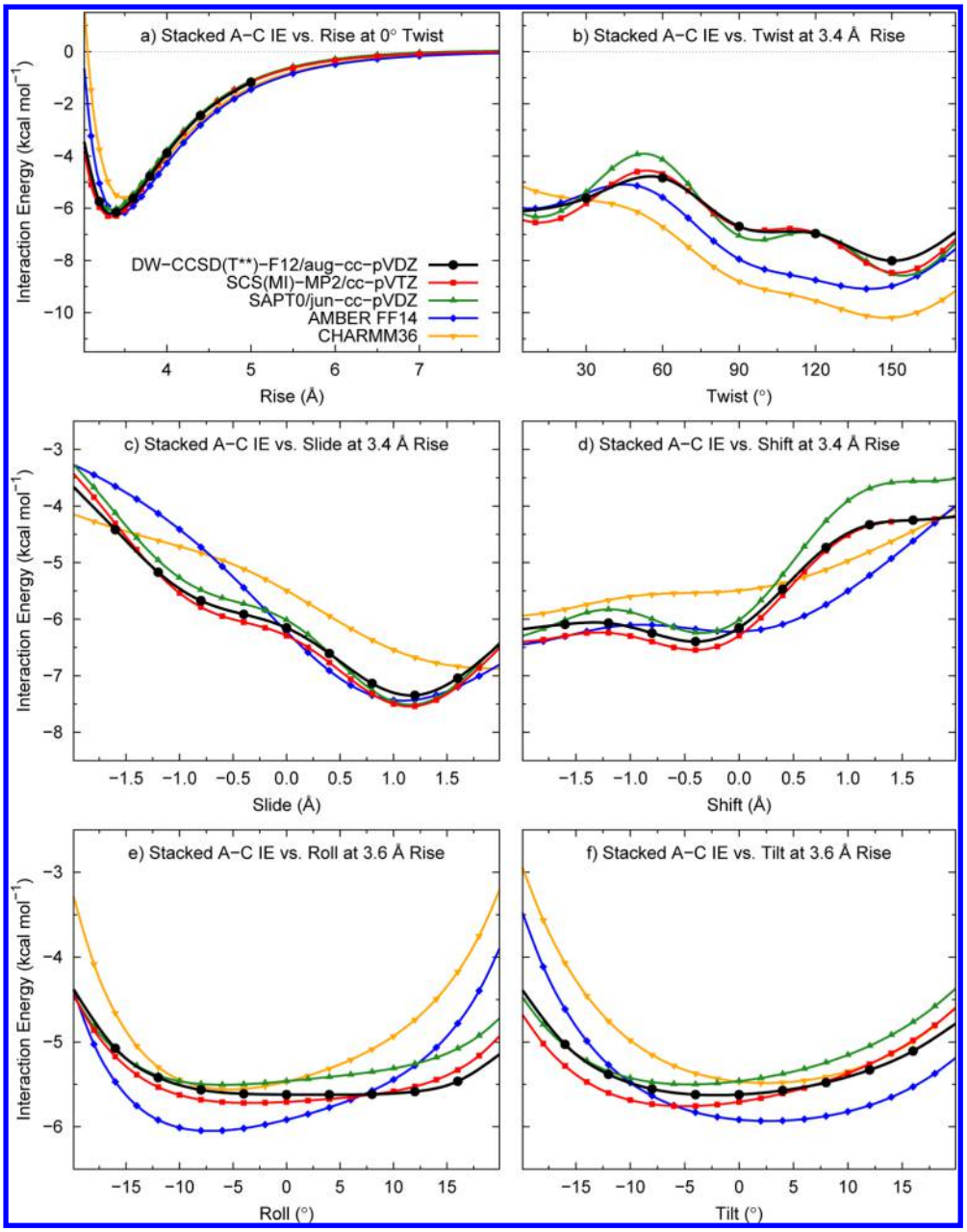

Figure 3. Comparison of stacking interaction energy computed for potential energy surfaces across varying nucleic acid helical parameters[35,36] for the stacked adenine−cytosine dimer. Helical parameters include three rotations (Twist, Roll, Tilt) and three translations (Rise, Slide, Shift) in the *Z*, *Y*, and *X* directions, respectively. Model chemistries include silver standard[13] DW-CCSD(T**)-F12/aug-cc-pVDZ, pewter standard[13] SCS(MI)-MP2/cc-pVTZ, bronze SAPT standard[14] SAPT0/jun-cc-pVDZ, and molecular mechanics force fields AMBER and CHARMM.

compared to ab initio methods, consistent with charge penetration errors.

Variations in IE versus Twist are dominated by electrostatics, which are presumably dominated by dipole−dipole interactions in these neutral, near-planar molecules. AMBER and CHARMM reproduce qualitative trends versus Twist, but they vary considerably more from SCS(MI)-MP2 and DW-CCSD(T**)-F12 than was the case versus Rise. This may result from limitations in reproducing the correct electrostatics using only atom-centered point charges. The overall MAE relative to SCS(MI)-MP2/cc-pVTZ across all stacked base pairs for the Rise−Twist PES is 1.4 kcal mol^{-1} for both AMBER and CHARMM, indicating reasonable performance. Maximum errors are 12.3 and 9.9 kcal mol^{-1} for AMBER and CHARMM, respectively, with these errors occurring at close contact ($R_{ij} \leq 0.8R_o$) points near the repulsive wall of the PES. Only points that have a below-zero SCS(MI)-MP2 reference energy are included in the above MAE, avoiding any excessive errors due to regions of the PES that are not explored much at physiological temperatures. Without this restriction, maximum errors become more than an order of magnitude larger at these very short-range contact geometries (Rise was considered down to 3.0 Å, compared to a typical value of 3.2−3.4 Å in B-DNA).[38,39]

The central two panels of Figure 3 plot two 1D slices of the Slide−Shift PES for adenine−cytosine, which cover both dimensions of horizontal in-plane translations of the cytosine relative to adenine at a constant Rise of 3.4 Å. Here, we again

DOI: 10.1021/acs.jctc.5b00588
J. Chem. Theory Comput. 2015, 11, 4197−4204

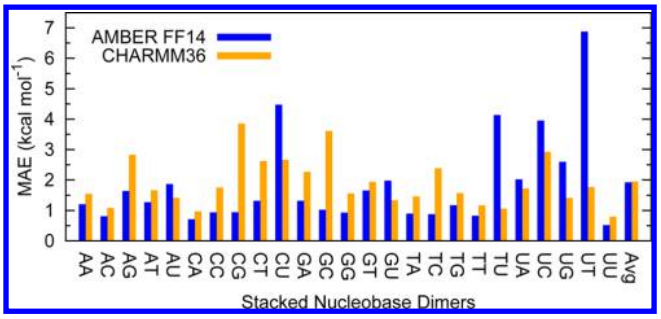

Figure 4. Mean absolute error (MAE) of selected molecular mechanics methods (AMBER and CHARMM) relative to SCS(MI)-MP2/cc-pVTZ reference stacking energies for all 25 stacked canonical nucleobase pairs. Values are the simple average of three subset MAE, one for each of three 2D potential energy scans over helical parameters (Rise−Twist, Slide−Shift, and Tilt−Roll). Due to extremely large errors in some parts of the PES, only structures that have an attractive (≤0 kcal mol^{-1}) reference IE are included in the averages.

see that AMBER and CHARMM retain the correct qualitative shape of the PES with minor varying deviations. The MAE's of 0.4 and 0.5 kcal mol^{-1} of AMBER and CHARMM relative to SCS(MI)-MP2/cc-pVTZ for the adenine−cytosine base stack are among the smallest MAE's for any pair of bases for this PES. The AMBER and CHARMM MAE's over all pairs of bases for the Slide−Shift PES are 1.4 and 1.6 kcal mol^{-1}, respectively.

The final two panels of Figure 3 plot the Tilt−Roll PES versus Tilt and Roll while the opposing parameter is zero and at a constant Rise of 3.6 Å (increased +0.2 Å relative to Figure 3c,d to decrease steric clashes). AMBER and CHARMM perform very well near the center of these plots, as both Tilt and Roll approach zero, approximating a structure from panel (a) versus Rise. Significant amounts out-of-plane rotation in panels (e) and (f) quickly result in several kcal mol^{-1} of deviation away from DW-CCSD(T**)-F12/aug-cc-pVDZ values.

For each 2D PES (Rise−Twist, Shift−Slide, and Tilt−Roll), we computed the MAE (across all points on the 2D PES) of the AMBER and CHARMM stacking energies vs SCS(MI)-MP2/cc-pVTZ ab initio reference values. These results are reported in the Supporting Information. The simple average of these three MAE values (each 2D PES MAE weighted equally) is reported for each possible pair of stacked nucleobases in Figure 4 (along with the average over all stacked dimers).

Although the Tilt−Roll PES is reasonable for A−C (as just discussed above), several other stacked dimers, especially homodimers CC, GG, and UU, have significant steric clashes for larger values of Tilt and/or Roll, resulting in enormous errors at these geometries. These errors can become far greater than 100 or even 1000 kcal mol^{-1} in such instances. For this reason, and as already mentioned above in our discussion of close contacts in the Rise−Twist PES, we have universally discluded points with a repulsive (positive) reference IE from reported error statistics. For the three problematic stacked dimers, this choice results in no usable points for the Tilt−Roll PES average. Thus, for these three dimers, the averages over the MAE of the three 2D PES's reported in Figure 4 are actually averages over only the Rise−Twist and Slide−Shift MAE.

As shown in Figure 4, the average MAE's over all stacked nucleobase dimers are 1.9 and 2.0 kcal mol^{-1} for AMBER and CHARMM, respectively. Maximum errors for individual dimers range from as low as 8 to >100 kcal mol^{-1}. Errors typically decrease as structures resemble those more typically observed in B-DNA and increase rapidly during steric clashes and deviations from parallel stacking. For most dimers, AMBER displays a smaller MAE than CHARMM, but in 7 of 25 dimers, the reverse is true, most notably for uracil containing dimers CU, TU, and UT.

3.3. Energy Component Comparisons between QM and MM for Stacking Energies between Two Base Pairs.

So far, our examination of the stacking energies between two nucleobases indicates fairly good performance by AMBER and CHARMM at geometries approaching those found in B-DNA, with larger errors (sometimes unphysically large) found during our scans of the six helical geometry parameters when close contacts occur. In this section, we move from computing the stacking energies between two nuclebases to computing the stacking energies between two base pairs. These systems (involving four nucleobases simultaneously) are too large for conventional CCSD(T) computations, but our benchmarking studies above indicate that SCS(MI)-MP2/cc-pVTZ and SAPT0/jun-cc-pVDZ stacking energies are fairly accurate, and both methods are applicable to systems of this size. Here, we will focus on SAPT0/jun-cc-pVDZ, which will allow us to examine how the stacking energy breaks down into contributions from electrostatics, exchange-repulsion (sterics), induction (polarization), and London dispersion forces. We recently published an analysis of all 10 unique DNA base pair steps using this level of theory, with a focus on understanding the fundamental physics of π-stacking in DNA and how it varies depending on the constituent base pairs.[30] Here, we use these energy components to better understand why CHARMM and AMBER fail in those cases where they exhibit large errors vs the QM results. Each hydrogen-bonded base pair was treated as a monomer for the purposes of the SAPT0 computations so that the SAPT0 interaction energies are stacking energies.

We computed CHARMM, AMBER, and SAPT0/jun-cc-pVDZ stacking energies for all 10 canonical DNA nucleobase steps as a function of the six helical parameters (Rise, Twist, Roll, Tilt, Slide, Shift). In this section, we vary only one helical parameter at a time, with the other five parameters fixed at their average NDB crystallographic value for that base pair step. The SAPT0 computations provide electrostatic, exchange-repulsion, induction, and dispersion energy components. AMBER and CHARMM contain force field terms that are not necessarily directly equivalent to these SAPT components, but nevertheless, for the sake of comparison, we plot these analogous terms to gain insight into the origins of the discrepancies between the MM and QM stacking energies. Note that standard (nonpolarizable) AMBER and CHARMM do not contain terms analogous to the SAPT induction component; however, this term contributes relatively little to nucleobase stacking except at short distances. The complete results from all of these comparisons are provided in the Supporting Information. As a representative example, Figure 5 presents SAPT0, CHARMM, and AMBER stacking energy components for the AC:GT base pair step as a function of Rise.

MM dispersion (R^{-6} term) is significantly overbound (too attractive) relative to SAPT0, with exchange (R^{-12} term) being insufficiently repulsive but by a lesser magnitude. Electrostatics performs qualitatively well until Rise < 4 Å, where charge penetration effects[28−30] take over, and MM is extremely underbound, with MM electrostatics remaining fairly flat and SAPT0 electrostatics becoming exponentially attractive due to overlap of diffuse electron clouds. These terms combine for a

DOI: 10.1021/acs.jctc.5b00588
J. Chem. Theory Comput. 2015, 11, 4197−4204

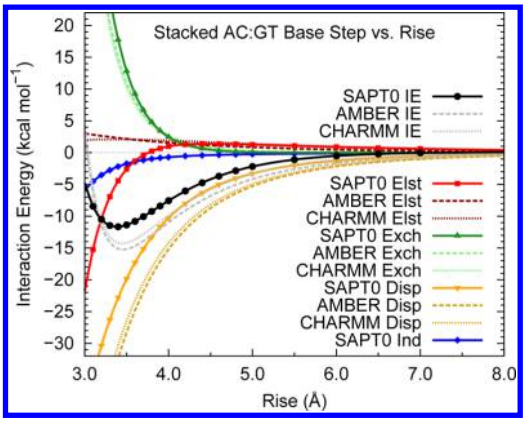

Figure 5. Comparison of stacking interaction energy components computed for potential energy curve versus Rise (at average B-DNA crystallographic values for other helical parameters) for the AC:GT base step. Interaction energy components include electrostatics, exchange-repulsion, and dispersion for molecular mechanics force fields AMBER and CHARMM. Also included for SAPT0/jun-cc-pVDZ is induction, which does not have a direct analogue in nonpolarizable AMBER or CHARMM.

cancellation of error that results in a total MM IE that is ∼3−4 kcal mol^{-1} overbound relative to SAPT0 at the minimum IE but with a similar value of the equilibrium value of Rise. These results are consistent with the previous results of Hobza and co-workers[31] in which the AMBER IE's for 10 B-DNA steps were within ∼2 kcal mol^{-1} of roughly estimated CCSD(T)/CBS values near their equilibrium structures. The energy component comparison in Figure 5 is qualitatively similar to previous comparisons of SAPT and MM for the parallel-displaced benzene dimer,[27] in which significant underestimation of repulsive exchange cancels out significant underbinding by MM electrostatics (MM electrostatics for benzene dimer in the geometries considered has the wrong sign). Base steps vary in whether their long-range MM electrostatics is attractive or repulsive, but in all cases, charge penetration takes over at short range (<4 Å) and MM electrostatics becomes very underbound relative to SAPT0 electrostatics.

Note also that at very short range (<3.2 Å) the MM IE's quickly become underbound, as the errors in the MM electrostatics term overwhelm the errors in the MM dispersion term. For all 10 base steps versus Rise, MM dispersion has the largest errors at long range where MM electrostatics errors are small. The electrostatics errors then rapidly increase below 3.5 Å Rise and are the largest source of error for all steps at 3.0 Å Rise. This leads to the previously discussed behavior observed in the Tilt−Roll PES's for nucleobase dimers, where very large MM IE errors [relative to the SCS(MI)-MP2/cc-pVTZ reference IE] are observed during close contacts. In Figure 5 at 3.0 Å Rise, the SAPT0 IE is still atractive (−5 kcal mol^{-1}), whereas the AMBER and CHARMM IE's are repulsive by +5 and +3 kcal mol^{-1}, respectively, with a much larger derivative versus Rise for the MM models; this is consistent with our observations of occasional errors >10 kcal mol^{-1} for CHARMM and AMBER stacking energies of nucleobase dimers even in regions where the SAPT0 and SCS(MI)-MP2 IE remained attractive.

4. CONCLUSIONS

MM models have previously demonstrated difficulty in reproducing high-quality ab initio interaction energy (IE) data for noncovalent interactions in small π-stacked systems like the benzene dimer.[27] Here, we seek to address whether similar difficulties are encountered for π-stacking interactions between nucleobases. A thorough comparison of stacking interactions between two nucleobases in canonical B-DNA geometries and across PES scans indicates that the AMBER and CHARMM models perform qualitatively correctly across the majority of the energetically accessible PES. Performance is best at canonical B-DNA geometries, where IE mean absolute errors below 1 kcal mol^{-1} versus silver standard DW-CCSD(T**)-F12/aug-cc-pVDZ are achieved. Average errors are more typically in the 2 kcal mol^{-1} range versus pewter standard SCS(MI)-MP2/cc-pVTZ for PES's that span the parameter space of these stacked bases. Maximum errors can become extreme (>10 kcal mol^{-1}), even for structures with attractive ab initio reference interaction energies, with MM models becoming very repulsive too quickly during close contacts due to insufficiently attractive MM electrostatics. This problem may be difficult or even impossible to solve without adding explicit terms to the force field to account for charge penetration. For the PES of base step IE's vs Rise, SAPT0 and MM electrostatics agree at long range until charge penetration effects take over at Rise < 4.0 Å. MM IE's at minimum energy vs Rise (∼3.4 Å) are typically overbound (too attractive) by 2−6 kcal mol^{-1} relative to bronze SAPT standard SAPT0/jun-cc-pVDZ. As Rise continues to decrease, the errors in the oversimplified MM point-charge model vs SAPT electrostatics grow very rapidly because of the exponential increase in the charge penetration contribution.

The present results indicate that careful parametrization and current MM potential functions are sufficient to provide fairly accurate stacking energies for nucleobases near typical B-DNA geometries, primarily through a cancellation of errors in the various terms making up the force field. However, this cancellation of errors does not persist as the PES is sampled more widely, even if we restrict consideration to geometries with an attractive stacking energy. This suggests that current functional forms are simply too limited to provide good results at a wide range of geometries, even if one were to attempt reparameterization.

Fortunately, some work has been done on including charge penetration terms in general force fields, including the quantum mechanical polarizable force field (QMPFF),[45,46] the Gaussian electrostatic model (GEM)[47−49] and related Gaussian multipole model (GMM),[50] the effective fragment potential (EFP),[51,52] and recent force-fields by Schmidt and co-workers,[53,54] as well as recent additions to the AMOEBA force field.[55] The present work suggests that these improved force fields should be much more robust than point-charge-based force fields for distorted geometries of DNA and RNA with close interatomic contacts.

■ ASSOCIATED CONTENT

Supporting Information

The Supporting Information is available free of charge on the ACS Publications website at DOI: 10.1021/acs.jctc.5b00588.

Full description of the process/program used to generate geometries; data tables with all numerical values for Figures 2−5; graphs analogous to Figure 3 for all 25 stacked base−base interactions (data tables attached); and analogous content to Figure 5 for all 10 base steps with attached data tables (PDF).

DOI: 10.1021/acs.jctc.5b00588
J. Chem. Theory Comput. 2015, 11, 4197−4204

All geometries used for computations as xyz files (ZIP and ZIP).

AUTHOR INFORMATION

Corresponding Author

*E-mail: sherrill@gatech.edu.

Funding

This work was supported by a research grant provided by the United States National Science Foundation (Grant No. CHE-1300497).

Notes

The authors declare no competing financial interest.

ACKNOWLEDGMENTS

T.M.P. thanks Meserret Zekarias for helpful assistance. Computational resources at the Center for Computational Molecular Science and Technology are supported through an NSF-CRIF award (Grant No. CHE-0946869) and by Georgia Tech. The authors also thank Georgia Tech for computational resources provided by the PACE cluster.

REFERENCES

(1) Meyer, E. A.; Castellano, R. K.; Diederich, F. *Angew. Chem., Int. Ed.* **2003**, *42*, 1210−1250.
(2) Salonen, L. M.; Ellermann, M.; Diederich, F. *Angew. Chem., Int. Ed.* **2011**, *50*, 4808−4842.
(3) Saenger, W. *Principles of Nucleic Acid Structure*; Springer-Verlag: New York, 1984.
(4) Yanson, I. K.; Teplitsky, A. B.; Sukhodub, L. F. *Biopolymers* **1979**, *18*, 1149−1170.
(5) Nir, E.; Kleinermanns, K.; de Vries, M. S. *Nature* **2000**, *408*, 949−951.
(6) Riley, K. E.; Pitoňák, M.; Jurečka, P.; Hobza, P. *Chem. Rev.* **2010**, *110*, 5023−5063.
(7) Marshall, M. S.; Burns, L. A.; Sherrill, C. D. J. *J. Chem. Phys.* **2011**, *135*, 194102.
(8) Demovicova, L.; Hobza, P.; Řezáč, J. *Phys. Chem. Chem. Phys.* **2014**, *16*, 19115−19121.
(9) Smith, D. G. A.; Jankowski, P.; Slawik, M.; Witek, H. A.; Patkowski, K. *J. Chem. Theory Comput.* **2014**, *10*, 3140.
(10) Raghavachari, K.; Trucks, G. W.; Pople, J. A.; Head-Gordon, M. *Chem. Phys. Lett.* **1989**, *157*, 479−483.
(11) Burns, L. A.; Marshall, M. S.; Sherrill, C. D. *J. Chem. Theory Comput.* **2014**, *10*, 49−57.
(12) Lee, T. J.; Scuseria, G. E. In *Quantum Mechanical Electronic Structure Calculations with Chemical Accuracy*; Langhoff, S. R., Ed.; Kluwer Academic Publishers: Dordrecht, 1995; pp 47−108.
(13) Burns, L. A.; Marshall, M. S.; Sherrill, C. D. *J. Chem. Phys.* **2014**, *141*, 234111.
(14) Parker, T. M.; Burns, L. A.; Parrish, R. M.; Ryno, A. G.; Sherrill, C. D. *J. Chem. Phys.* **2014**, *140*, 094106.
(15) Burns, L. A.; Vázquez-Mayagoitia, Á.; Sumpter, B. G.; Sherrill, C. D. *J. Chem. Phys.* **2011**, *134*, 084107.
(16) Řezáč, J.; Riley, K. E.; Hobza, P. *J. Chem. Theory Comput.* **2011**, *7*, 2427−2438.
(17) Distasio, R. A., Jr.; Head-Gordon, M. *Mol. Phys.* **2007**, *105*, 1073−1083.
(18) Jeziorski, B.; Moszynski, R.; Szalewicz, K. *Chem. Rev.* **1994**, *94*, 1887−1930.
(19) Hohenstein, E. G.; Sherrill, C. D. *J. Chem. Phys.* **2010**, *132*, 184111.
(20) Hohenstein, E. G.; Parrish, R. M.; Sherrill, C. D.; Turney, J. M.; Schaefer, H. F. *J. Chem. Phys.* **2011**, *135*, 174107.
(21) Halgren, T. A. *J. Comput. Chem.* **1996**, *17*, 490−519.
(22) MacKerell, A. D.; Bashford, D.; Bellott, M.; Dunbrack, R. L.; Evanseck, J. D.; Field, M. J.; Fischer, S.; Gao, J.; Guo, H.; Ha, S.; Joseph-McCarthy, D.; Kuchnir, L.; Kuczera, K.; Lau, F. T. K.; Mattos, C.; Michnick, S.; Ngo, T.; Nguyen, D. T.; Prodhom, B.; Reiher, W. E.; Roux, B.; Schlenkrich, M.; Smith, J. C.; Stote, R.; Straub, J.; Watanabe, M.; Wiorkiewicz-Kuczera, J.; Yin, D.; Karplus, M. *J. Phys. Chem. B* **1998**, *102*, 3586−3616.
(23) Cornell, W. D.; Cieplak, P.; Bayly, C. I.; Gould, I. R.; Merz, K. M.; Ferguson, D. M.; Spellmeyer, D. C.; Fox, T.; Caldwell, J. W.; Kollman, P. A. *J. Am. Chem. Soc.* **1995**, *117*, 5179−5197.
(24) Hess, B.; Kutzner, C.; van der Spoel, D.; Lindahl, E. *J. Chem. Theory Comput.* **2008**, *4*, 435−447.
(25) Jorgensen, W. L.; Tirado-Rives, J. *J. Am. Chem. Soc.* **1988**, *110*, 1657−1666.
(26) Halgren, T. A. *Curr. Opin. Struct. Biol.* **1995**, *5*, 205−210.
(27) Sherrill, C. D.; Sumpter, B. G.; Sinnokrot, M. O.; Marshall, M. S.; Hohenstein, E. G.; Walker, R. C.; Gould, I. R. *J. Comput. Chem.* **2009**, *30*, 2187−2193.
(28) Stone, A. J. *The Theory of Intermolecular Forces*; Oxford University Press: Oxford, 1996.
(29) Hohenstein, E. G.; Duan, J.; Sherrill, C. D. *J. Am. Chem. Soc.* **2011**, *133*, 13244−13247.
(30) Parker, T. M.; Hohenstein, E. G.; Parrish, R. M.; Hud, N. V.; Sherrill, C. D. *J. Am. Chem. Soc.* **2013**, *135*, 1306−1316.
(31) Šponer, J.; Jurečka, P.; Marchan, I.; Luque, F. J.; Orozco, M.; Hobza, P. *Chem. - Eur. J.* **2006**, *12*, 2854−2865.
(32) Becke, A. D. *J. Chem. Phys.* **1993**, *98*, 1372−1377.
(33) Kendall, R. A.; Dunning, T. H.; Harrison, R. J. *J. Chem. Phys.* **1992**, *96*, 6796−6806.
(34) Turney, J. M.; Simmonett, A. C.; Parrish, R. M.; Hohenstein, E. G.; Evangelista, F. A.; Fermann, J. T.; Mintz, B. J.; Burns, L. A.; Wilke, J. J.; Abrams, M. L.; Russ, N. J.; Leininger, M. L.; Janssen, C. L.; Seidl, E. T.; Allen, W. D.; Schaefer, H. F.; King, R. A.; Valeev, E. F.; Sherrill, C. D.; Crawford, T. D. *WIREs Comput. Mol. Sci.* **2012**, *2*, 556−565.
(35) El Hassan, M. A.; Calladine, C. R. *J. Mol. Biol.* **1995**, *251*, 648−664.
(36) Lu, X.-J.; Babcock, M. S.; Olson, W. K. *J. Biomol. Struct. Dyn.* **1999**, *16*, 833−843.
(37) Dickerson, R. E.; Bansal, M.; Calladine, C. R.; Dickmann, S.; Hunter, W. N.; Kennard, O.; von Kitzing, E.; Lavery, R.; Nelson, H. C. M.; Olson, W. K.; Saenger, W.; Shakked, Z.; Sklenar, H.; Soumpasis, D. M.; Tung, C.-S.; Wang, A. H.-J.; Zhurkin, V. B. *EMBO J.* **1989**, *8*, 1−4.
(38) Perez, A.; Noy, A.; Lankas, F.; Luque, F. J.; Orozco, M. *Nucleic Acids Res.* **2004**, *32*, 6144−6151.
(39) Berman, H. M.; Olson, W. K.; Beveridge, D. L.; Westbrook, J.; Gelbin, A.; Demeny, T.; Hsieh, S. H.; Srinivasan, A. R.; Schneider, B. *Biophys. J.* **1992**, *63*, 751−759.
(40) Wang, J.; Cieplak, P.; Kollman, P. A. *J. Comput. Chem.* **2000**, *21*, 1049−1074.
(41) When calculating interaction energies between rigid monomers, only nonbonded parameters affect the resulting final value. The nonbonded parameters from AMBER FF95 remain unchanged, despite many updates of bonded parameters. Thus, the interaction energies for these nucleobase dimers should be equivalent for all AMBER versions from FF95 to FF14. FF14 is chosen as the label to indicate that the parameters chosen are still valid in present versions.
(42) Foloppe, N.; MacKerell, A. D., Jr. *J. Comput. Chem.* **2000**, *21*, 86−104.
(43) Marshall, M. S.; Sherrill, C. D. *J. Chem. Theory Comput.* **2011**, *7*, 3978−3982.
(44) Werner, H.-J.; Knowles, P. J.; Manby, F. R.; Schütz, M.; Celani, P.; Knizia, G.; Korona, T.; Lindh, R.; Mitrushenkov, A.; Rauhut, G.; Adler, T. B.; Amos, R. D.; Bernhardsson, A.; Berning, A.; Cooper, D. L.; Deegan, M. J. O.; Dobbyn, A. J.; Eckert, F.; Goll, E.; Hampel, C.; Hesselmann, A.; Hetzer, G.; Hrenar, T.; Jansen, G.; Köppl, C.; Liu, Y.; Lloyd, A. W.; Mata, R. A.; May, A. J.; Tarroni, R.; Thorsteinsson, T.; Wang, M.; Wolf, A. *MOLPRO*, version 2010.1, a package of ab initio programs. http://www.molpro.net.
(45) Donchev, A. G.; Ozrin, V. D.; Subbotin, M. V.; Tarasov, O. V.; Tarasov, V. I. *Proc. Natl. Acad. Sci. U. S. A.* **2005**, *102*, 7829−7834.

DOI: 10.1021/acs.jctc.5b00588
J. Chem. Theory Comput. 2015, 11, 4197−4204

(46) Donchev, A. G.; Galkin, N. G.; Pereyaslavets, L. B.; Tarasov, V. I. *J. Chem. Phys.* **2006**, *125*, 244107.
(47) Cisneros, G. A.; Piquemal, J. P.; Darden, T. A. *J. Chem. Phys.* **2005**, *123*, 044109.
(48) Cisneros, G. A.; Piquemal, J.-P.; Darden, T. A. *J. Chem. Phys.* **2006**, *125*, 184101.
(49) Duke, R. E.; Starovoytov, O. N.; Piquemal, J.-P.; Cisneros, G. A. *J. Chem. Theory Comput.* **2014**, *10*, 1361−1365.
(50) Elking, D. M.; Cisneros, G. A.; Piquemal, J.-P.; Darden, T. A.; Pedersen, L. G. *J. Chem. Theory Comput.* **2010**, *6*, 190−202.
(51) Flick, J. C.; Kosenkov, D.; Hohenstein, E. G.; Sherrill, C. D.; Slipchenko, L. V. *J. Chem. Theory Comput.* **2012**, *8*, 2835−2843.
(52) Gordon, M. S.; Fedorov, D. G.; Pruitt, S. R.; Slipchenko, L. V. *Chem. Rev.* **2012**, *112*, 632−672.
(53) McDaniel, J. G.; Yu, K.; Schmidt, J. R. *J. Phys. Chem. C* **2012**, *116*, 1892−1903.
(54) McDaniel, J. G.; Schmidt, J. R. *J. Phys. Chem. A* **2013**, *117*, 2053−2066.
(55) Wang, Q.; Rackers, J. A.; He, C.; Qi, R.; Narth, C.; Lagardere, L.; Gresh, N.; Ponder, J. W.; Piquemal, J.; Ren, P. *J. Chem. Theory Comput.* **2015**, *11*, 2609−2618.

DOI: 10.1021/acs.jctc.5b00588
J. Chem. Theory Comput. 2015, 11, 4197−4204